Radiation Measurements 57 (2013) 19–28

Contents lists available at SciVerse ScienceDirect

Radiation Measurements

journal homepage: www.elsevier.com/locate/radmeas

Superheated emulsions and track etch detectors for photoneutron measurements

A. Di Fulvio [a,b,*], C. Domingo [c], M. De San Pedro [c], E. D'Agostino [d], M. Caresana [e], L. Tana [f], F. d'Errico [a,b]

[a] Dipartimento di Ingegneria Meccanica, Nucleare e della Produzione, Università di Pisa, Largo L. Lazzarino 2, Pisa I-56125, Italy
[b] Yale University School of Medicine, 333 Cedar Street, New Haven, CT 06511, USA
[c] Departament de Física, Universitat Autònoma de Barcelona, E-08193 Bellaterra, Spain
[d] Radioprotection, Dosimetry and Calibration Unit, Belgian Nuclear Research Center, Belgium
[e] Politecnico di Milano, CESNEF, Dipartimento di Energia, via Ponzio 34/3, 20133 Milano, Italy
[f] Santa Chiara University Hospital, via Roma 67, Pisa I-56125, Italy

HIGHLIGHTS

- Selection criteria of measurement techniques for photoneutron dosimetry.
- We developed newer readout methods for the selected techniques.
- We employed chosen methods in realistic in-phantom irradiations.
- Increasing measurement accuracy and readout throughput.

ARTICLE INFO

Article history:
Received 19 June 2012
Received in revised form
18 November 2012
Accepted 26 November 2012

Keywords:
Neutron detectors
Superheated emulsions
Superheated drop detectors
Track etch PADC detectors

ABSTRACT

This paper describes the criteria behind the selection of neutron detection techniques for photoneutron dosimetry as well as the methods adopted to obtain dosimetric readouts. The work was conducted within the framework of Working Group 9 (WG9 Radiation Protection Dosimetry in Medicine), coordinated by the European Radiation Dosimetry Group (EURADOS). WG9 research aims at estimating the risk of second cancer induction due to radiation therapy. Therefore, a comprehensive experimental programme was devised to measure doses received by non-target organs-at-risk (OAR) during radiation therapy. The techniques described in this work were selected and used for the neutron dosimetric assessment during in-phantom simulations of clinical prostate radiotherapy treatments, carried out in three European facilities. Non-conformal standard fields were used as a common reference between different facilities.

Performing neutron measurements near linacs is a complex task, because of the intense pulsed photon primary field. Therefore, photon insensitive dosimeters such as superheated emulsions (SE) and solid state nuclear track detectors (SSNTD) were chosen. Their readout procedures were carefully assessed. Methods were developed to count the large number of tracks and bubbles in SE. These are described in detail in the present work, along with a brief introduction to the detector physics.

1. Introduction

Fast neutron contamination of the x-ray and electron beams used in radiation therapy poses a significant problem of undue exposure for the patient, which has been recognized since the 1950s (Laughlin et al., 1951). Advanced radiotherapy techniques, i.e. intensity-modulated radiotherapy (IMRT), stereotactic and volumetric-modulated arc therapy (VMAT), have achieved many goals in terms of conformal dose distribution and treatment effectiveness (Wolff et al., 2009), but have not solved the intrinsic problem of neutron contamination. The structural complexity of treatment machines may indeed increase the neutron leakage probability (Zytkovicz et al., 2007). A dosimetric characterization of mixed photoneutron fields continues to be needed. This requires specific techniques for assessment of the neutron equivalent dose from photoneutrons in a clinical environment, during realistic treatments, where the dominant photon component can saturate the response of many laboratory neutron counters. For this reason,

* Corresponding author. Yale University School of Medicine, 333 Cedar Street, New Haven, CT 06511, USA. Tel.: +1 475 201 7312; fax: +1 203 785 6534.
E-mail address: angela.difulvio@yale.edu (A. Di Fulvio).

1350-4487/$ – see front matter © 2012 Elsevier Ltd. All rights reserved.
http://dx.doi.org/10.1016/j.radmeas.2012.11.022

photon insensitive superheated emulsions and solid state nuclear track detectors are good candidates for out-of-field neutron radiation therapy dosimetry. In-phantom measurements are also made possible, because of the relatively small detector dimensions. These devices do not require an external power supply and their readout can be performed at the end of the irradiation. Passive operation allows a response which is independent of the neutron flux, so that detectors can be placed either within the target volume, where high neutron fluxes can be achieved or at a distance from the primary axis of the beam, where high detection sensitivity is required. As a matter of fact, both SE and track detectors, along with their readout methods, feature high sensitivity, which makes it possible to detect minimum doses of the order of a microsievert.

This paper describes the criteria behind the selection of neutron detection techniques for photoneutron dosimetry as well as the methods adopted to obtain dosimetric readouts. The work was conducted within the framework of Working Group 9 (WG9 Radiation Protection Dosimetry in Medicine), coordinated by the European Radiation Dosimetry Group (EURADOS).

The energy response of these detectors needs also to be evaluated with regard to photoneutron spectra in medical accelerators, where photoneutrons are directly generated by high energy photon interactions with the x-ray target and the beam flattening filter. To this component, an evaporation term, with a Maxwellian energy distribution, is superimposed (Tosi et al., 1991). A further thermal neutron component is generated by multiple scattering events within the construction materials and either within the phantom or patient. In this work, a water filled poly-methyl methacrylate BOMAB-like phantom was used (Di Fulvio et al., 2013).

The superheated emulsion detectors consist of a suspension of fluoro-/halo- carbon droplets, dispersed in a tissue equivalent gel. Importantly, the detector response compares well with the fluence to kerma equivalent conversion factor for fast neutrons: this is a key SE feature for dosimetric applications in medical linac fields. Two types of SE detectors have been considered in this work: superheated drop detectors (Università di Pisa, SDD - UNIPI) and bubble damage detectors (BDT and BD-PND), produced by Bubble Technology Industries (BTI) ®. SE response is temperature dependent: response energy thresholds of around 200 keV are achieved for both SDDs and BD-PND at 27 °C operating temperature. These thresholds do not cause a significant dose underestimation, as the contribution of thermal neutrons to in-phantom dose is mainly due to gamma rays, which are produced by the absorption reactions on hydrogen atoms. The contribution of thermal neutrons is less than 5% of the total dose (Agosteo et al., 1993). This value is below the overall measurement uncertainty, thus it can be neglected at a first approximation.

On the other hand, nuclear track dosimeters, also known as track etch detectors, record recoil charged particles originated by neutron interactions inside the detector itself or in materials, used as converters, placed on top of the detector. Neutron dosimeters developed at Universitat Autònoma de Barcelona (UAB) and at Politecnico di Milano (Italy) were considered. The first are based on a Poly-allyl-diglycol carbonate (PADC) track detector, covered with polyethylene, which produces protons from fast neutrons through elastic (n,p) scattering, and Makrofol, flattening the high energy response of the dosimeter in the 0.5–5 MeV energy range. An additional Nylon layer sensitizes the detector to thermal neutrons, via the $^{14}N(n,p)^{14}C$ capture reaction. The response function of the sensitized detector matches well the fluence to dose equivalent conversion coefficient in the fast neutron energy range. However, it overestimates the dose equivalent conversion coefficient in the thermal range, where it follows the $^{14}N(n,p)^{14}C$ reaction cross section (Domingo et al., 2013). Therefore PADC detectors are suitable for in-phantom photoneutron measurements assuming that their readout is weighted by an appropriate position dependent factor, which accounts for the actual impinging neutron spectrum on the detectors.

The Radiator Degrader Neutron Spectrometer (RDNS) developed at Politecnico di Milano consists of a polyethylene (PE) radiator and an aluminium degrader of variable thickness, placed on top of a PADC sheet detector. The basic principle of this approach is that the recoil protons originating from the radiator material must fall within a definite energy range to penetrate the aluminium layer and damage the PADC surface. Different response functions are achieved by the RDNS, by using multiple PE and aluminium thicknesses. After neutron irradiation, a set of data is obtained, which is acquired by means of different detectors, one for each combination of thicknesses. This kind of SSNTD is thus capable of spectral measurements by unfolding the detector response function kernel with the acquired data set. The low energy threshold of RDNS response functions is around 200 keV, so they are preferred for in-field measurements of linac generated photoneutrons, where the direct fast component dominates.

2. Basic features of superheated emulsions and readout methods for out-of-field neutron dose measurements

The application of superheated emulsions in practical neutron detectors was first introduced by (Apfel, 1979). Nowadays, the effectiveness of these devices has been widely recognized from both the scientific and technological point of view. This is confirmed by their classification among neutron detectors by ISO (in preparation) and ICRU (Deng, 2002). Their working principle has been widely studied after Seitz (Seitz, 1958) and is based on the kinetic energy transfer by the charged secondaries, produced by neutrons interactions, to the emulsion drops, hosted in an inert matrix.

Recoil ions are generated by neutron interactions inside the emulsion. They lose their energy by interacting with the surrounding material in a relatively small distance of the order of tenths of microns, at room temperature (d'Errico, 2001). They can thus induce a phase transition, from liquid to gas, of the metastable emulsion, which consists of micrometric-size liquid drops, kept in a superheated state. As the macroscopic effect of neutron interaction is the evaporation of fluoro/halo-carbon emulsion drops, these devices are also known as bubble detectors. Their response has been proven to match well the standard dosimetric conversion coefficients (d'Errico et al., 1998b; Vanhavere et al., 1998). For this reason, bubble detectors have been used for neutron dosimetric purposes, in the range between a few 100 keV to about 10 MeV.

This energy range includes the photoneutron spectrum which is present around high-energy radiotherapy x-ray beams. Therefore, superheated emulsions are often used for the dosimetric characterization of linac-generated photoneutron fields. Passive bubble counting methods, based on volumetric readout and visual inspection, have been used extensively for measurements in photoneutron clinical fields (d'Errico et al., 1998a). The two bubble counting methods presented in this work have been applied to two kinds of bubble detectors: SDDs, developed at Yale and Pisa University and BDT and BD-PND, produced by BTI® and provided by SCK·CEN (Fig. 1). The main features of these two bubble detectors are reported in Table 1.

They mainly differ in the host matrix composition, which is water based in SDDs and polymeric in BDTs and BD-PNDs. A unified parameterization of superheated emulsions is made possible with the reduced superheat factor. Reduced superheat S is defined as follows, where T is the operating temperature:

$$S = (T - T_b)/(T - T_c) \quad (1)$$

Fig. 1. SDDs (left) and BD-PND (right).

T_b and T_c are the boiling and critical temperature at a given pressure, respectively (d'Errico, 2013).

Octafluorocyclobutane (C-318) emulsion is used in SDDs, and its reduced superheat at room temperature is 0.26. Reduced superheat has been reported since it is a thermodynamic ratio and an index of how close the operating temperature is to the critical one. It is unity when the two temperatures T_b and T_c are equal. Reduced superheat is also significant for the detector energy response. As a matter of fact, the higher the degree of superheat, the lower the energy required to generate vapor bubbles. A reduced superheat less than 0.4 implies a response energy threshold higher than 200 keV, so that the detector is selectively sensitive to fast neutrons. Since a scattered low-energy neutron component is expected for in-phantom measurements, BDT detectors have also been used, which are sensitive to thermal neutrons via the exergonic ^{6}Li$(n,\alpha)^3$H capture reaction in a ^{6}Li compound dispersed throughout the polymeric matrix.

Bubble detectors are very suitable for the measurement of neutrons in mixed fields, since they are insensitive to the intense dominant photon flux of this radiation field. C-318 has a moderate degree of superheat at room temperature. C-318 droplet vaporization requires a linear energy transfer (LET) of about 300 keV/μm over the critical radius of the bubble. This energy deposition pattern was shown to be one order of magnitude higher (d'Errico, 2001) than the LET of high energy photoelectrons (>1 keV). C-318 based SDDs were irradiated with ^{137}Cs γ-rays and proven to be completely insensitive to photons at room temperature (d'Errico, 2001). The BD-PND detector photon insensitivity was also tested and confirmed by means of a variety of gamma sources, i.e. a ^{60}Co radiotherapy treatment unit (Waller et al., 2003).

SDDs and BTI® detector volumes are slightly different (Table 1 and Fig. 1), nevertheless their diameter is comparable; thus allowing the detectors to be inserted into plastic channels, as in the BOMAB-like phantom used in WG9 experimental measurements (d'Errico et al., 2013). Moreover, their cylindrical geometry guaranteed a two-axis measurement isotropy.

Neutron detectors were irradiated in reference and standard clinical radiotherapy fields, as also detailed in Di Fulvio et al., 2013, for photon doses ranging from 2 to 10 Gy. After irradiation and readout, a pressure higher than vapor tension was applied to condense evaporated drops to the liquid superheated state. A complete SDD recompression takes less than 5 s at a pressure of 7 atm, applied by an external hydraulic torque. BDTs and BD-PNDs recompression was instead carried out by means of their built-in screw-cap.

2.1. Optical read-out method

So far, the most effective integral measurements of the number of bubbles in SDDs were carried out either by measuring the gel volume increase or by visual inspection. Given the success of studies on the 3-D dose distributions in neutron-sensitive superheated emulsions via optical tomography (d'Errico et al., 2008), a scattered light based bubble detection device has been recently developed.

This consists of a light-tight enclosure holding the superheated emulsions, which is illuminated from the bottom by three infra-red, 15° half-emission angle LEDs. The scattered light is therefore sensed by three 980 nm focused planar photodiodes, placed at 120° along the detector walls. The transducer system estimates the number of bubbles by measuring the signal current induced in the photodiodes by scattered light.

After verifying the monotonic increase of scattered light as a function of the number of bubbles, a maximized sensitivity configuration has been found (d'Errico and Di Fulvio, 2011). The output photocurrent not only allowed scattered-light readings which were virtually independent of the bubble-formation position inside the detector, but which also increased uniformly for each evaporated bubble, because of the diameter homogeneity of mono-dispersed drops. The electronic device, acquiring and processing the light-induced signal, is microcontroller-based. A high impedance input transresistive low-noise amplifier provides front-end amplification and filtering of the integrated output photocurrent. The voltage signal so obtained is digitized by means of a 14 bit resolution ADC. A further digital mobile-average filtering is then operated by the microcontroller itself. The amount of detected light is converted either to the actual number of bubbles or neutron dose and is displayed on an LCD module. A thermistor sensor has also been introduced in order to implement a digital thermal compensation, where necessary.

The system also automatically memorizes a background signal for each detector, due to the variable spatial distribution of the liquid drops, and then subtracts it from the actual measurement.

Because of the high sensitivity of the system, which discriminates a single bubble, dose measurements with a resolution between 2 and 5 μSv were achievable.

2.2. Image recognition software applied to bubble counting

A different bubble counting method has been developed for BDT and BD-PND detectors. The optical readout device was not

Table 1
Comparison of superheated emulsion detectors.

	SDD	BD-PND & BDT	
Energy range	800 keV–20 MeV	200 keV–15 MeV	Thermal (1/v for epithermal)
Composition	Halocarbon C-318	Chlorofluorocarbon R-12	R-12 (plus ^{6}Li compound)
Sensitivity (bubbles μSv^{-1})	0.2 and 0.5 (average) for two detector sets	0.03–3.0 (average)	2.7 (average)
Dose range (μSv)	From 1 to 5000/2000 for two detector sets	1–5350	1.1–112
Size	L 40–Ø 18 mm	L 116–Ø 19 mm	L 123–Ø 19 mm
Recompression method	External apparatus	Integrated assembly	Integrated assembly

applicable in this case because the BDT and BD-PND emulsion holder vial is longer than that for the SDDs (Table 1) and the bubble diameter is less homogeneous. Bubble counting was thus carried out by means of image recognition software, developed in Matlab®(The MathWorks Inc., Natick, MA, 2009), which analyses detector pictures, recognizes the bubbles and counts them. These functions were mainly achieved by using the Hough transform, which will be briefly introduced in this section.

After applying a standard Sobel high-pass edge detector filter, the Hough algorithm was implemented to recognize circular shapes. At first, this transform was applied to the automated analysis of bubble chamber photographs (Bastien and Dunn, 1971); more recently its generalized form has been widely used for the recognition of shaped objects, particularly when their boundaries are described by analytic equations.

Before applying the transform, the equation describing the real object (i.e. dashed circle in Fig. 2) has to be known; it is $r^2 = (x-a)^2 + (y-b)^2$ in the present case, where r is the radius and a and b are the circle center coordinates in the x–y plane. Each point of the real object, which has been highlighted by the edge detector filter, is then mapped in the parameter Hough space, as a function of the shape parameters (a, b and r in this case). For each point, a three dimensional set of circumferences will be allowed to exist, as represented in Fig. 2, where the circumference radius has been kept constant for representational simplicity in the two dimensional plane. This procedure is iterated for all the points. The parameter Hough space is then quantized into finite interval accumulator cells, whose score increases with the cell parameter's recurrence, i.e. points belonging to the same circumference. The undetermined problem is then solved by considering the parameter plane score statistics: in this case points with scores higher than a fixed threshold have been selected.

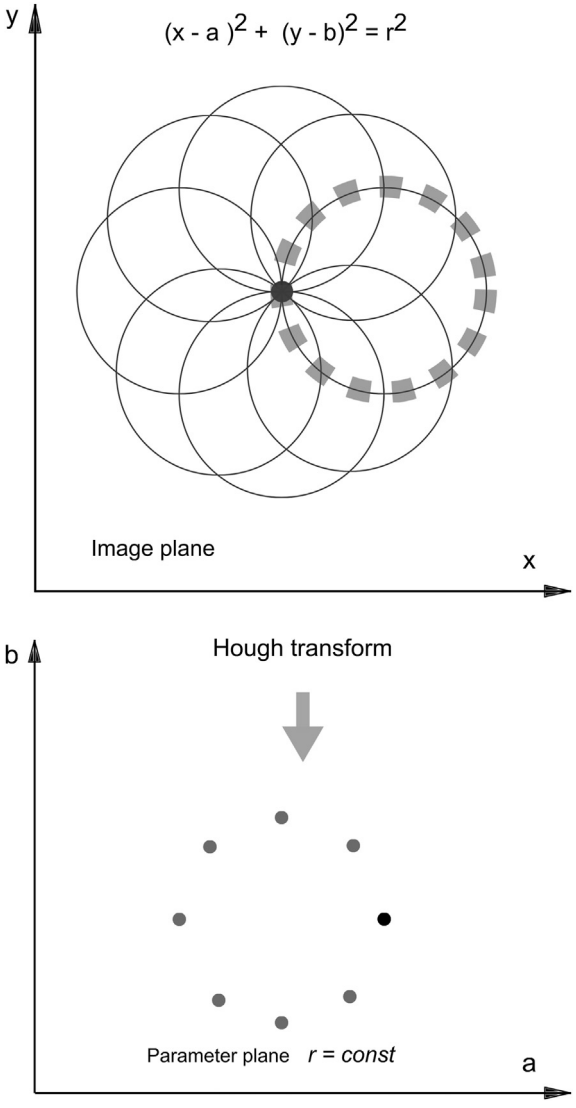

Fig. 2. Hough transform: basic principle for the representation of circular shapes.

By setting a suitable threshold, the algorithm is relatively insensitive to gaps in the boundaries, as well as to image noise, which is typically due to picture blurring. The implemented algorithm was checked by means of test bubble images, with a known number of randomly distributed circles. A blurring Gaussian filter was then subsequently applied, increasing the filter matrix dimension, which dramatically increased blurring and negatively affected bubble resolution.

Since a sharp grayscale image features a bimodal gray level distribution (Castelman, 1979), the ratio between the area below the two principal peaks and the total peak was taken as a blurring parameter. The closer to unity the parameter, the less the blurring. Eight blurring levels were chosen, with blurring parameter between 1 (no blurring) and 0.92. The maximum error made by the recognition software was 2%. In real bubble detector images, the blurring parameter minimum value is approximately 0.94. An example of an image of a real vial is shown in Fig. 3.

In any case, the error due to overlapping bubbles was unavoidable; it was mainly overcome by acquiring at least two pictures per each detector, from at least two angular views (0–90°), and by limiting radiation doses so that the number of evaporated bubbles was kept well below 200. The simple approach adopted here consisted of comparing multiple images related to the same detector and choosing the picture with the highest number of bubbles, considered to be the least affected by overlapping phenomena. Where it was possible to recognize hidden bubbles, they were manually added to the final count.

2.3. Detector calibration, dose calculation and uncertainties

Each SE detector was individually calibrated, in order to obtain a calibration coefficient specific for each detector. A measurable physical quantity close to the absorbed dose at a point, given

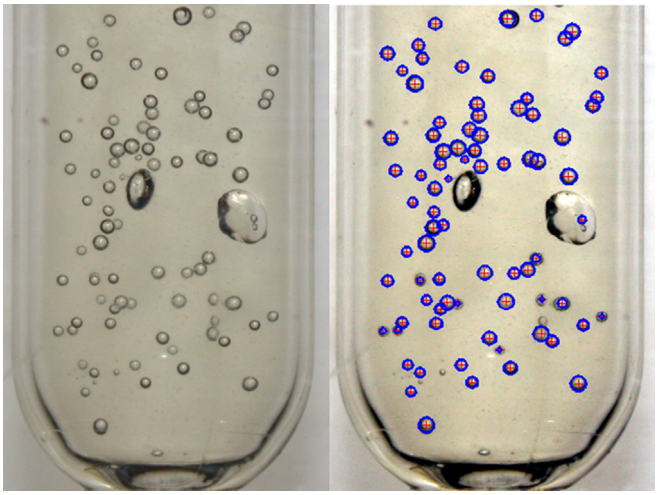

Fig. 3. Software segmentation and counting applied to a real BD-PND bubble detector image.

charged particle equilibrium, is the tissue kerma. The energy response of SE detectors corresponds well with the fluence to kerma equivalent conversion coefficient (Vanhavere et al., 1998, d'Errico, 2001), which is the average tissue kerma per unit neutron fluence, weighted by the quality factor of the neutron charged secondaries (Caswell et al., 1980). The dosimetric response of SE detectors can thus be considered ideal and calibration coefficients can be applied to a variety of neutron fields, regardless of the spectrum.

Superheated drop detectors have been calibrated at the University of Pisa, by means of a 1.1 GBq AmBe neutron source. Since detector response is sensitive to the operating temperature, the calibration procedure has been performed at 27 °C, the average value measured inside the clinical radiotherapy facilities. Calibration has been performed in air, according to ISO 8529 guidelines (ISO, 1998).

Although a specific geometric correction model is still lacking for cylindrical detectors, such as SE vials, according to a recent study at the National Physical Laboratory (NPL) (Taylor, 2010), a source to detector distance should be at least four times the detector diameter. In the present case, given a detector diameter of 1.8 cm and a detector height of 4 cm, the source to detector distance was set to 50 cm, which is sufficient to assume a broad and parallel field at the detector position, whilst keeping the counting rate acceptable.

The shadow cone method, as described in ISO 8529-2 (ISO, 2000), has been applied during calibration, in order to evaluate the neutron scattered component. Two scattering contributions, represented in Fig. 4, may be distinguished: the first one is the inscatter which increases the detector count. This is due to neutrons scattered by air or by the structure of the irradiation room, towards the detector. The second contribution is the outscatter, which includes all those neutrons scattered from their original path which would have crossed the detector, and causes a decreasing detector count. While the first component is directly measured with the shadow cone method, the second is evaluated with the air-attenuation factor F_A, according to ISO 8529-2 annex C (ISO, 2000). A 50 cm long shadow cone, 20 cm iron and 30 cm borate polyethylene, suitably designed for superheated drop detectors, has been used. The transmission of the primary AmBe flux through the cone has been simulated by means of Monte Carlo MCNPX code and results in a 2% transmission.

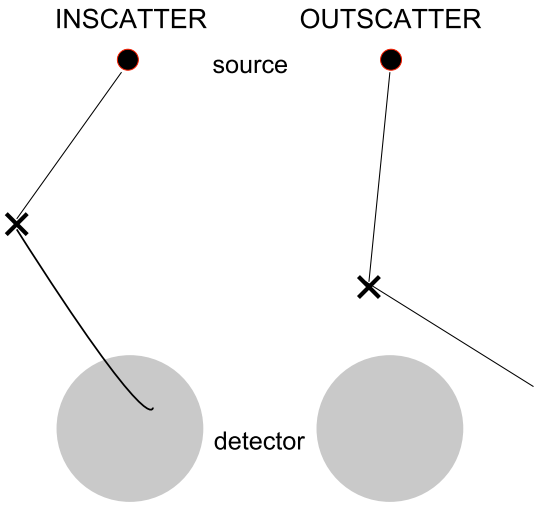

Fig. 4. Neutron inscatter and outscatter.

The shadow cone method has been implemented by deducing M_C (the measured count corrected for all external effects) from Equation (2), where M_S and M_T are detector readings obtained with and without shadow cone respectively.

$$(M_T - M_S)F_A = M_C \tag{2}$$

In Equation (2) the air attenuation coefficient F_A depends on the source to detector distance and on nitrogen and oxygen total neutron cross section (ISO, 2000). M_C has been subsequently used to obtain the fluence response (R_Φ) in the AmBe field from Equation (3), where B is the neutron source strength, $F(\Omega)$ is the source anisotropy correction factor (ISO 8529, 1998) and l the source to detector distance.

$$R_\Phi = M_C\left(\frac{BF(\Omega)}{4\pi l^2}\right)^{-1} \tag{3}$$

The kerma equivalent response coefficient (R_K), in terms of bubbles per unit kerma, has been then obtained by Equation (4), using the fluence to kerma conversion coefficient for AmBe (k_ϕ), by weighting the kerma equivalent factor (Siebert and Schuhmacher, 1995) with the normalized AmBe spectrum (ISO, 1998).

$$R_K = \frac{R_\Phi}{k_\phi} \tag{4}$$

The calibration has been repeated several times for each detector, in order to verify their stability and to estimate detector readout accuracy. Two sets of detectors have been used, with a different amount of C-318, resulting in two kerma equivalent response coefficients of 0.2 (±0.03) and 0.5 (±0.08) bubble μSv^{-1}. A dead time correction factor was not required since integral dose measurements were executed at the end of each irradiation.

The previously described method has been detailed since it is a general one and could be applied to any kind of neutron detector. BTI® BDPND bubble detectors were calibrated, with similar analytic procedures, by placing them on the front side of a 30 × 30 × 15 cm^3 ICRU slab phantom (ICRU, 1998) and irradiating with a Cf-252 source at the SCK-CEN. BDT detectors were calibrated at a thermal reactor beam at the BR1 reactor at the SCK-CEN. BDPND and BDT have been calibrated in terms of personal dose equivalent $H_p(10)$.

Kerma equivalent response calibration coefficients were then obtained by multiplying BDPND and BDT $H_p(10)$ calibration coefficients by 1.2 and 3.4 respectively (Vanhavere et al., 1998). In BTI® detectors, a compressible material, inserted on top of the vial, is able to adjust for sensitivity changes due to temperature fluctuations, within the 20–37 °C operational range (Tume et al., 1998). Despite this temperature compensation method, sensitivity has been shown to increase up to 50% with increasing operating temperature and about 15% with detector age, after repeated irradiations (Vanhavere et al., 1996), in the 20–37 °C temperature range. However, the sensitivity has been shown to be well compensated for temperatures lower than 27 °C, which is the average operating temperature inside the linac irradiation room (Vanhavere et al., 1996).

The main source of uncertainty for bubble detectors is the response of sensitivity to temperature. Equation (5) is a general formula to compensate measured kerma K by detector thermal sensitivity; α is the thermal sensitivity positive coefficient, while ΔT is the difference between the operating temperature and the calibration temperature; α varies between 0.05 and 1.3 $°C^{-1}$ in the 15–40 °C temperature range. In the present case, since operation and calibration temperatures were comparable, the term ΔT is negligible and no correction is needed for both BTI and UNIPI detectors.

$$K = \frac{(1 - \alpha\Delta T)M_T}{R_K} \quad (5)$$

The temperature variation was strictly controlled for both SDDs and BTI® detectors. However a conservative 1 standard deviation (SD) uncertainty of 10% was added to the measured value in order to take into account eventual temperature fluctuations of ±1 °C inside the treatment room, during irradiations. Counting stability in terms of dose equivalent energy response as a function of spectral hardness was measured in several experimental intercomparisons for SDD (d'Errico et al., 1996) and was estimated to be within 13% (1 SD in %) of the reference value for the energy range of photoneutron fields produced by linacs and radionuclide sources. An additional error in the counting of the number of bubbles with the described readout devices has been estimated as less than 5% (1 SD in %), for typical readings of at least 100 bubbles. Hence, this uncertainty analysis implies an overall error of about 18% (1 SD in %). An analogous dose equivalent response accuracy has been also measured for BTI® detectors during calibration in Am–Be radionuclide fields, including the errors related to the conversion coefficient (about 3%), to scatter corrections (about 1%) (Vanhavere et al., 1998) and to the counting device.

3. Basic features of track etch detectors and readout methods for out-of-field neutron dose measurements

Among plastic solid state materials used as nuclear track detector, PADC is considered the most sensitive (Fews and Henshaw, 1983). In fact, a relatively low irradiation dose per PADC chain disruption is required, since PADC has a limited capability for chain crosslinking after radiation damage. Radiation is thus capable of generating defects in PADC, which permanently remain on the plastic foil. Moreover, optical transparency and homogeneity are two relevant features which are suitably exploited for track counting.

Certain insulating materials were observed to become more chemically etchable after interaction with charged particles (Fleischer et al., 1975). Chemical etching enlarges tracks and makes them visible to the standard optical microscope and easy to count. This is the basic physical principle on which nuclear track etch detectors rely. Radiation interactions within these materials result at first in local shallow damages, called latent-damage tracks. Damage becomes chemically etchable if energy higher than a characteristic threshold level is imparted to the track by radiation. Plastic materials have a sufficiently low threshold which is usually referred to as the minimum unrestricted linear energy transfer (LET) of the interacting charged particle, necessary to create a track. PADC, among other plastic materials, has the lowest threshold unrestricted LET of 5 keV μm^{-1} for unit-density tissue (Zhou et al., 2007). Dose estimation for PADC detectors is based on the existing relationship between the LET and the damage caused by radiation. Moreover, PADC composition is $C_{12}H_{18}O_7$, similar to tissue. The chemical etching procedure has also to be carefully designed to give an accurate estimation of the dose, since low range charged particles could disappear after the etching, even if their LET still exceeds the PADC sensitivity threshold. Two etching procedures have been optimized for neutron dosimetry purposes and will be described in the next section.

A remarkable feature of track etch detectors is the insensitivity to high kinetic energy, low LET particles, such as photons. This therefore makes these detectors particularly suitable for neutron measurements in mixed fields.

At the UAB, extensive research has been performed in recent years to develop a PADC based neutron dosimeter with a relatively flat energy response from thermal to fast neutrons. To achieve this aim, a convenient set of neutron converting materials was placed in front of the detector, whose elements generate secondary charged particles, produced by neutron interactions. The actual configuration of the dosimeter (Garcia et al., 2005), from top to bottom, is composed of a polyethylene layer (3 mm) and a Makrofol polycarbonate layer (300 μm), which are both fast neutron converters via elastic scattering with hydrogen. These are followed by a Polyamide Nylon 6 layer (100 μm), acting as converter for thermal neutrons through the $^{14}N(n,p)^{14}C$ reaction, which releases a 626 keV proton, easily recorded by the underlying PADC layer (500 μm). The bottom layer is a methacrylate holder (5 mm).

The detector response for personal dosimetry was evaluated experimentally with ISO sources and realistic neutron fields, as specified in ISO 8528-2 (ISO, 2000) and ISO 12789 (ISO, 2008), at the Institut de Radioprotection et de Sureté Nucléaire (IRSN, Cadarache, France) facilities, as well as with quasi-monoenergetic neutron beams at the Van der Graaf accelerator of the Institute for Reference Materials and Measurements (IRMM) of the European Commission Joint Research Centre (JRC), Geel (Belgium) (Domingo et al., 2009). It was found that the response in terms of fluence varies from about 10^{-5} tracks per neutrons at ~70 keV up to a maximum of $2 \cdot 10^{-4}$ tracks per neutron at 2 MeV and practically vanishes at energies >20 MeV.

Estimating neutron equivalent doses at several points for in-phantom irradiations is a complicated task since the neutron energy spectrum at the measurement point is unknown and the irradiation configuration is non-standard. Specific strategies have been adopted within WG9 to estimate out-of-field neutron dose during clinical simulations of prostate radiotherapy using a BOMAB-like phantom and are described in the next sections.

The radiator degrader neutron spectrometer developed at Politecnico di Milano, is based on a 25 × 25 mm^2 PADC sheet, 1.4 mm thick, supplied by Intercast (Parma, Italy). This is covered by an aluminum degrader foil with a radiator PE clad layer. These have both variable thicknesses in the range of 10–500 μm and 0.2–2 mm respectively, which are overlapped to obtain 15 different PE/Al thickness combinations and the same number of response functions (Caresana et al., 2012b). A neutron spectrum is derived by unfolding the detector response function kernel with the acquired data set by means of the iterative GRAVEL algorithm.

3.1. Etching and counting procedures

After irradiation, the PADC sheets are electrochemically etched with a standard procedure described in García et al. (2005). Track density is later determined through a semi-automatic process (Amgarou et al., 2001).

Different etch procedures of PADC detectors exist, which consist of enlarging latent-damage tracks by attacking the detector with a strong acid or alkaline solution. The etching speed of this solution is 10 times higher for latent-tracks than for normal surfaces. The etched tracks so obtained may be visualized with a standard optical microscope.

In electrochemical etching (ECE), an alternating voltage is applied across the detector between two platinum electrodes. Electrochemical etching is typically preferred to standard chemical etching for neutron sensitive detectors, because it enhances the response to low energy neutrons (Tommasino et al., 1984).

According to the etching procedure used at UAB, PADC sheets were etched using 6N KOH aqueous solution at 60.0 ± 0.1 °C, at first by applying a 20 kV cm^{-1} RMS at 50 Hz for 5 h and then by increasing the frequency to 2 kHz for a shorter interval time of 1 h (Garcia et al., 2005). Finally, a post-etching of 15 min was performed. The etching process is handled by a computer-controlled

multifunction Data Acquisition System, which generates a highly stable, low-voltage sinusoidal signal, whose amplitude and frequency are selectable by computer. The low-voltage signal is subsequently amplified by a high-speed high-voltage power amplifier with a fixed 1000 gain. The high voltage signal so obtained is thus supplied to the ECE unit at the required frequency (de San Pedro, 2011). Electrochemical etching has many advantages over a chemical method, since the alternating electric field causes a tree shape track propagation, into large tracks, mainly independent of the original depth of the track and thus on the energy of charged secondaries. The low 50 Hz frequency is necessary in the first stage of the etching procedure to confine the tree-like track propagation within a small region, otherwise the whole detector bulk would be saturated. In contrast to the chemical approach, this procedure does not allow energy discrimination, but it guarantees that low LET interacting charged particles may also be counted. In fact, in chemical etching, shallower tracks created by low-energy (<100 keV) protons are likely to be over-etched in a shallower layer of the detector and disappear in the final etching stage, when the 5–15 microns detector upper layer is removed from the surface (Tommasino et al., 1984).

However, the chemical etching procedure is sometimes preferred because, upon treatment, each track remains as a hole, which is the tip of the cone created by the etching agent at the latent track. The size of the pit created by the neutron recoils depends upon the direction of the interacting particles and restricted energy loss (REL). REL equals the linear energy transfer without the contribution of the delta electrons with energy higher than 350 eV, which deposit their energy far from the ionizing particle trajectory and thus do not contribute to the track formation. By measuring the size and geometrical features of the track, it is possible to determine the energy and type of charged recoil particle which created the track and so estimate the energy of the neutron which generated the recoil inside the PE converting layer (Caresana et al., 2010). The chemical etching is thus an unavoidable choice whenever reaction energetics information is needed to perform spectrometry, as in the case of RDNS. As a matter of fact these detectors are etched, after irradiation, in a NaOH 6.25 mol aqueous solution at 98 °C for 90 min.

After etching, tracks in PADC-UAB detectors were counted by means of a semi-automatic system designed at UAB, which consists of a commercial photo-slide scanner with high optical resolution (9600 dpi). The scanner incorporates counting software, based on Matlab® (The MathWorks Inc., Natick, MA, 2009) and suitably developed for track counting and capable of discriminating well overlapping tracks (de San Pedro, 2011).

The etched RDNS plastics were analyzed with a commercial reader Politrack (Miam, Milano Italy), developed at the Politecnico di Milano, which is able to count the number of pits, as well as to calculate many pit parameters, such as pit area and perimeter and pit minor and major axes (Miam, 2012). From the pit parameters the Politrack derives physical quantities such the REL (Caresana et al., 2012a).

3.2. Detector calibration, dose calculation and uncertainties

The electrochemical etching procedure does not allow direct information about the energy deposited by the interacting radiation to be deduced. It is thus possible to assign neutron fluence values from the net track density calibration only if an *a-priori* knowledge of the neutron energy spectrum is given. Calibration of PADC dosimeters for personal dosimetry is commonly performed in terms of personal dose equivalent H_p, referring to external irradiation of an individual. The H_p response function of the UAB-PADC dosimeters was obtained from irradiations in reference fields (Domingo et al., 2013) and experimentally verified in workplaces at specific points (i.e. in the treatment room of a medical linac), where spectra and dosimetric quantities were measured by means of a Bonner sphere spectrometer (Bedogni et al., 2013). Nevertheless, in-phantom neutron fields are not suitably characterized by H_p.

Specific calibration irradiations of PADC dosimeters were carried out at the Physikalisch-Technische Bundesanstalt (PTB) primary neutron facility to simulate the neutron field inside a phantom. Free-in-air neutron irradiations were carried out in order to characterize the response of the detectors in terms of fluence. Different filters have been used to suitably modify the primary spectrum and make it similar to linac-generated photoneutron spectra. Three different spectra have been produced (Fig. 5), all of them presenting a fast neutron component (0.5–1 MeV) and a low energy peak, resembling photoneutron spectra (Zimbal, 2009). The spectra were derived using the MCNP code and calculations were verified by means of measurements with a Bonner sphere spectrometer (Kluge, 1998). As PADC response is strongly angle dependent (Domingo et al., 2013), the PADC response was evaluated for normally incident neutrons, as well as for isotropic irradiation. Details of the irradiation spectra and the calibration procedure are described by Sánchez-Doblado et al. (2012). Table 2 shows the calibration factors in terms of fluence obtained for both directional (normal incidence) and isotropic irradiations. Reference values for ambient dose equivalent $H^*(d)$, i.e. the dose equivalent at a depth d in the reference ICRU spherical phantom, were also provided for the PTB exposures, so that calibration factors in terms of ambient dose equivalent could be calculated (Table 2). All uncertainties displayed in Table 2 are derived from track counting statistics at a 1 SD level, combined with the fluence and ambient dose equivalent uncertainties provided by the PTB (Zimbal, 2009).

Calibration factors for the electrochemically etched UAB-PADC dosimeter differ significantly depending on the energy and angular distributions of the neutron field.

Computer simulations of photoneutron spectra inside an anthropomorphic phantom showed that the out-of-field contribution of the thermal neutron component to the total fluence increases with the distance from the isocentre (Sánchez-Doblado et al., 2012). For this reason, the type II spectrum provided by the PTB (Fig. 5) was considered a good approximation for the out-of-field energy distribution of neutrons inside the phantom. The type II spectrum provided by the PTB (Fig. 5) compares well with

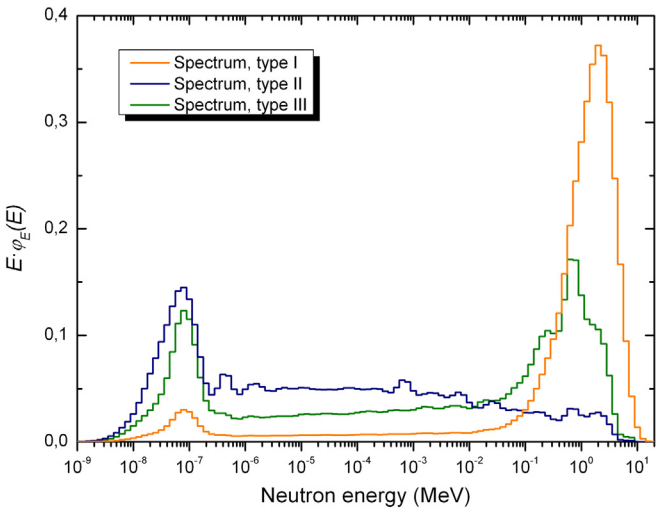

Fig. 5. Filtered spectra provided by the PTB and used for PADC calibration (Domingo et al., 2010).

Table 2
Calibration conversion factors for 3 different spectra: net track density per unit neutron fluence and per ambient dose equivalent for directional (normal incidence) and isotropic irradiation fields.

	Spectrum type I	Spectrum type II	Spectrum type III
Description	^{252}Cf source	^{252}Cf(D2O + Cd) + shadow block	^{252}Cf source + Shadow cone
Type	Fast	Epithermal + thermal	Fast + epithermal + thermal
p_t	0.052	0.312	0.211
p_e	0.103	0.592	0.380
p_f	0.845	0.097	0.409
f_{dir} (fluence response cm^{-2})	$(1.118 \pm 0.066) \times 10^{-4}$	$(4.65 \pm 0.48) \times 10^{-6}$	$(1.762 \pm 0.090) \times 10^{-5}$
f_{iso} (fluence response cm^{-2})	$(5.16 \pm 0.90) \times 10^{-5}$	$(2.15 \pm 0.24) \times 10^{-6}$	$(8.13 \pm 0.58) \times 10^{-6}$
h_{dir} (ambient dose equivalent response mSv^{-1})	361 ± 21	134 ± 14	140.4 ± 7.2
h_{iso} (ambient dose equivalent response mSv^{-1})	166 ± 13	61.7 ± 7.0	64.8 ± 4.6

p_t is the thermal fluence fraction, p_e is the epithermal fluence fraction, p_f is the fast fluence fraction, f_{dir} is the fluence response for normal incidence, f_{iso} is the fluence response for isotropic incidence, h_{dir} is the ambient dose equivalent response for normal incidence and h_{iso} is the ambient dose equivalent response for isotropic incidence.

the energy distribution of neutrons inside the phantom, as confirmed by computer simulations of photoneutron transport inside an anthropomorphic phantom (Sánchez-Doblado et al., 2012). The thermal component is also mostly isotropic, because of in-phantom and room scattering, whereas the fast and the epithermal neutrons are highly directional, since they come from the primary neutron radiation originating in the accelerator head.

The neutron dose equivalent at a point inside the phantom is evaluated from the energy fluence distribution Φ_E, the kerma factor k and the radiation quality factor Q (Equation (6)).

Φ_E is the product of the total fluence Φ and the unit energy distribution of fluence φ_E. The neutron dose equivalent can be expressed as in Equation (5), assuming an isotropic thermal component Φ_t and highly directional fast and epithermal component ($\Phi_{e,f}$).

$$\begin{aligned} H &= \int_E \Phi(E)k(E)Q(E)\mathrm{d}E = \Phi_t \int_{E_t} \varphi_E(E)k(E)Q(E)\mathrm{d}E_t \\ &\quad + \Phi_{e,f} \int_{E_{e,f}} \varphi_E(E)k(E)Q(E)\mathrm{d}E_{e,f} \\ &= C\left(\frac{p_t}{f_{iso}} \int_{E_t} \varphi_E(E)k(E)Q(E)\mathrm{d}E_t \right. \\ &\quad \left. + \frac{p_e+p_f}{f_{dir}} \int_{E_{e,f}} \varphi_E(E)k(E)Q(E)\mathrm{d}E_{e,f}\right) = \frac{C}{F} \end{aligned} \quad (6)$$

In Equation (6), p_t, p_e and p_f are the fractional contribution of thermal, epithermal and fast neutrons respectively to the total fluence. f_{iso} and f_{dir} are the fluence calibration coefficients for isotropic and directional incidence (Table 2), C is the measured track density in the detector (tracks cm^{-2}) and F is the resulting overall calibration coefficient in terms of neutron dose equivalent. For a type II spectrum, $F = 175$ tracks cm^{-2} mSv^{-1} inside the treatment target volume. An increased thermal component at points adjacent to the target volume leads to $F = 750$ tracks cm^{-2} mSv^{-1}. Far away from the irradiated volume, $F = 1162$ tracks cm^{-2} mSv^{-1} accounts for the attenuation of the fast component and the further reduction of the epithermal component.

The overall uncertainty of the calibration depends on both total track count and calibration coefficient uncertainties. This latter contribution results from the uncertainty associated with the calibration source fluence rate and the fluence to ambient dose equivalent conversion coefficients. This latter 1 SD uncertainty is about 5% (Kluge et al., 1997; Alberts, 1999). The neutron field quality fluence rate combined uncertainty is 4% (Kluge et al., 1997; Domingo et al., 2010). The counting statistics follow a Poisson distribution, so that the random error is the square root of the number of tracks observed. The variability of the etching process also negatively affects the measurement reproducibility. The UAB readout method has an intrinsic counting uncertainty less than ±10% (1 SD in %), achievable for dose equivalents not exceeding 75% of the maximum measurable value (≈50 smSv), so that overlapping of etched tracks is avoided (Garcia et al., 2005; NCRP, 2008). The dose equivalent used in calibration and measurement should thus be high enough to achieve a reasonable track count, but still guarantee track discrimination.

The uncertainty propagation of the different contributions determines an overall uncertainty between 20% and 40% (1 SD in %), which can be associated with the dose measured by electrochemical etched PADC detectors. Higher uncertainties refer to the spectral distribution of neutrons outside the irradiated volume, where the discrepancy between the calibration spectra and the actual spectra is larger.

A different approach is necessary for the calibration of a chemically etched SSNTD. As mentioned in the previous paragraph, the neutron elastic collisions with the hydrogen nuclei in the carbonate chains and in the radiator layer generate directly ionizing charged particles. The recoil protons from these collisions mimic well the actual conversion of the neutron energy to ionizing energy which occurs in tissue. For this reason, the equivalent dose can be derived from the number of tracks and their mean LET, without accounting for the impinging neutron spectrum. The mean LET of a particle, averaged over a track, can be deduced by knowing the ratio between track and bulk etching velocities, the etching duration and the track geometric parameters (Caresana et al., 2012a,b). The equivalent dose can be thus calculated as in Equation (7) (Caresana et al., 2012a,b). Equation (7) is valid in the absence of a PE radiator; otherwise a coefficient depending on the radiator thickness, the LET and the track angle should be introduced to compensate for the sensitivity increase due to the radiator.

$$H = \frac{1}{\rho} \cdot 1.602 \cdot 10^{-6} \cdot \sum_{i=1}^{n} \frac{\overline{\mathrm{LET}_i}}{\cos\vartheta_i} Q\left(\overline{\mathrm{LET}_i}\right) \quad (7)$$

In Equation (7), for n particles impinging on a unit area detector (1 cm^2), LET$_i$ is the mean linear energy transfer expressed in keV μm^{-1}, ρ is the density in g cm^{-3}, Q(LET$_i$) the quality factor as defined in ICRP 60 and θ the angle between the impinging particle and the direction normal to the detector surface. The factor $1.602 \cdot 10^{-9}$ is needed for energy unit conversion. Equation (7) allows the calculation of equivalent dose regardless of the neutron spectrum. Specific uncertainties affecting this measurement method are associated with the number of counted tracks, the value of the impinging angle of the particles and with the value of

LET averaged over the track length, which is about 10% (Caresana et al., 2012a,b). The lower number of variables to be controlled during the chemical etching, with respect to the electrochemical one, causes a lower overall 1SD uncertainty of about 20% (NCRP, 2008).

4. Conclusions

Practical methods of measuring in-phantom neutron doses have been presented in this work, which can also be useful for the characterization of emerging radiation therapy techniques and for their comparison in terms of the spurious neutron dose components.

Superheated emulsions and PADC nuclear track neutron detectors are intrinsically insensitive to photons and allow a passive and neutron flux-independent operation. These two main features, together with their relatively small size, lead to their selection for in-phantom measurements in photoneutron fields, generated by high energy photons in medical linacs. SE detectors also have a tissue-equivalent composition that avoids the creation of heterogeneities in the phantom and preserves charged particle equilibrium. The two methodologies allowed the three-dimensional mapping of in-phantom neutron dose profiles due to realistic treatment plans of prostate radiotherapy. The high sensitivity and dynamic range of the detectors allowed measurement with uncertainty as low as ±20% both in the target volume and in surrounding OARs.

In this work two methodologies have been presented, which allow reliable counting of the number of evaporated bubbles inside SE detectors. These two methods were successfully applied after in-phantom irradiations and proved to be good candidates to replace previously used time consuming strategies (i.e. visual inspection). Computer-based image recognition software has been exploited to count evaporated bubbles within BTI® detectors, while a stand-alone optoelectronic readout device has been used for SDD. These two strategies proved to be easy to use and sufficiently fast to give an immediate readout, which may be immediately converted into organ equivalent dose by knowing detector calibration coefficients. Both readout methods allowed single bubbles to be counted. This corresponds to a measurable resolution of the order of a few microsievert per unit absorbed dose of primary photons at the isocentre (μSv/Gy). Low neutron doses of microsieverts, normalized to the photon dose at the isocentre, can be thus measured after prolonged irradiation with good counting accuracy. Accuracies less than 10% were made possible by the large number of bubbles (~200) which can be counted before saturation.

The same viability has been reported for the high sensitivity electrochemical etching procedure developed for PADC detectors at UAB. This method, together with a semi-automatic process for track counting, allowed increased PADC foil processing and read-out speeds, which is crucial for the analysis of large numbers of detectors employed during in-phantom irradiations. RDNS application for dosimetry in linac-generated photoneutron fields was also proven to be feasible. Their energy response ranges from 200 keV up to 8 MeV and makes them very suitable for in-field measurement on the phantom surface, where the neutron spectrum is mainly fast and so the estimation of the dose can be very accurate. RDNS spectrometric capabilities may be used to measure the spectrum in reproducible points in the phantom. The acquired data will be then used as input for Monte Carlo particle transport codes to score the neutron dose in arbitrary positions inside the phantom and ultimately to validate other detector responses. An energy range response extension should be also considered, in order to detect thermal neutrons, whose contribution increases with off-axis distance.

Acknowledgment

Some of the research presented in this work was partially funded by MICINN (Ministerio de Ciencia e Innovación, Spain) project FIS2009-10634 and by the Catalan Research Management Agency (AGAUR) project 2009SGR-122.

References

Agosteo, S., Foglio Para, A., Maggioni, B., 1993. Neutron fluxes in radiotherapy rooms. Medical Physics. 20 (2 Pt 1), 407–414.
Alberts, Wolfgang G., 1999. Advanced Methods of Active Neutron Dosimetry for Individual Monitoring and Radiation Field Analysis (Ando). Ptb-n. Physikalisch-Technische Bundesanstalt, Braunschweig.
Amgarou, K., Font, L., Albarracin, D., Domingo, C., Fernandez, F., Baixeras, C., 2001. Semi-automatic evaluation system for nuclear track detectors applied to Radon measurements. Radiation Measurement 33 (2), 203–209.
Apfel, R., 1979. The superheated drop detector. Nuclear Instruments & Methods 162, 5.
Bastien, P.L., Dunn, L.A., 1971. Global transformations in pattern recognition of bubble chamber photographs. IEEE Transactions on Computers C 20 (9), 995–1001.
Bedogni, R., Domingo, C., Esposito, A., Gentile, A., García-Fusté, M.J., de-San-Pedro, M., Tana, L., d'Errico, F., Ciolini, R., Di Fulvio, A., 2013. Calibration of PADC-based neutron area dosemeters in the neutron field produced in the treatment room of a medical LINAC. Radiation Measurements 50, 78–81.
Caresana, M., Ferrarini, M., Pola, A., Agosteo, S., Campi, F., Porta, A., 2010. Study of a radiator degrader Cr39 based neutron spectrometer. Nuclear Instruments & Methods in Physics Research Section A–Accelerators Spectrometers Detectors and Associated Equipment 620 (2–3), 368–374.
Caresana, M., Ferrarini, M., Fuerstner, M., Mayer, S., 2012a. Determination of let in Padc detectors through the measurement of track parameters. Nuclear Instruments & Methods in Physics Research Section A–Accelerators Spectrometers Detectors and Associated Equipment 683, 8–15.
Caresana, M., Ferrarini, M., Porta, A., Campi, F., 2012b. Performance evaluation of a radiator degrader Cr39 based neutron spectrometer. Nuclear Instruments & Methods in Physics Research Section A–Accelerators Spectrometers Detectors and Associated Equipment 680, 155–160.
Castelman, K.R., 1979. Digital Image Processing. Prentice Hall, New-Jersey.
Caswell, R.S., Coyne, J.J., Randolph, M.L., 1980. Kerma factors for neutron energies below 30-Mev. Radiation Research 83 (2), 217–254.
de San Pedro, M., 2011. Millora del sistema de revelat, lectura i comptatge en dosimetria Neutrònica basat en detector plàstic CR-39. Diploma thesis (in catalan language). Universitat Autònoma de Barcelona.
d'Errico, F., 2001. Radiation dosimetry and spectrometry with superheated emulsions. Nuclear Instruments & Methods in Physics Research Section B 184, 26.
d'Errico, F., Alberts, W.G., Dietz, E., Gualdrini, G., Kurkdjian, J., Noccioni, P., Siebert, B.R.L., 1996. Neutron ambient dosimetry with superheated drop (Bubble) detectors. Radiation Protection Dosimetry 65 (1–4), 397–400.
d'Errico, F., Di Fulvio, A., 2011. Superheated emulsions for the detection of special nuclear material. Radiation Measurements 46 (12), 1690–1693.
d'Errico, F., Di Fulvio, A., Maryañski, M., Selici, S., Torrigiani, M., 2008. Optical readout of superheated emulsions. Radiation Measurements 43 (2–6), 432–436.
d'Errico, F., Nath, R., Silvano, G., Tana, L., 1998a. In vivo neutron dosimetry during high-energy Bremsstrahlung radiotherapy. International Journal of Radiation Oncology Biology Physics 41 (5), 1185–1192.
d'Errico, F., Nath, R., Tana, L., Curzio, G., Alberts, W.G., 1998b. In-phantom dosimetry and spectrometry of photoneutrons from an 18 Mv Linear accelerator. Medical Physics 25 (9), 1717–1724.
Deng, J. Icru Report 66: Determination of Operational Dose Equivalent Quantities for Neutrons. In: 66, edited by ICRU: Physics in Medicine and Biology., 2002.
Di Fulvio, A., Tana, L., Caresana, M., D'Agostino, E., de San Pedro, M., Domingo, C., d'Errico, F., 2013. Clinical Simulations of Prostate Radiotherapy using Bomab-like phantoms: results for neutrons. Radiation Measurements 57, 48–61.
Domingo, C., Amgarou, K., García-Fusté, M.J., de-San-Pedro, M., 2010. Personal Communication.
Domingo, C., de-San-Pedro, M., García-Fusté, M.J., Romero, M.T., Amgarou, K., Fernández, F., 2013. Estimation of the Response Function of a Padc Based Neutron Dosimeter in Terms of Fluence and Hp (10). Radiation Measurements 50, 82–86.
Domingo, C., Garcia-Fuste, M.J., Amgarou, K., Morales, E., Castelo, J., 2009. Measurements in quasi-monoenergetic neutron beams at the Ec-Irmm Van der Graaf accelerator for calibration of the Uab Padc based neutron dosimeter. Radiation Measurements 44 (9–10), 981–984.
Fews, A.P., Henshaw, D.L., 1983. Alpha-particle autoradiography in Cr-39: a technique for quantitative assessment of Alpha-Emitters in biological tissue. Physics in Medicine and Biology 28 (5), 459–474.
Fleischer, R.L., Price, P.B., Walker, R.M., 1975. Nuclear Tracks in Solids: Principles and Applications. University of California, Berkeley.
Garcia, M.J., Amgarou, K., Domingo, C., Fernandez, F., 2005. Neutron response study of two Cr-39 personal dosemeters with air and Nylon converters. Radiation Measurements 40 (2–6), 607–611.

ICRU, 1998. Conversion coefficients for use in radiological protection against external radiation. Icru. In: ICRU (Ed.), Report 57. ICRU Publications, Bethesda.
ISO, 1998. In: International Organization for Standardization (Ed.), Reference Neutron Radiations – Part 3: Calibration of Area and Personal Dosimeters and Determination of Response as a Function of Energy and Angle of Incidence, International Standard, pp. 8529–8533. Geneva.
ISO, 2000. In: International Organization for Standardization (Ed.), Reference Neutron Radiations – Part 2: Calibration Fundamentals of Radiation Protection Devices Related to the Basic Quantities Characterizing the Radiation Field. Geneva.
ISO, 2008. In: ISO (Ed.), Reference Radiation Fields – Simulated Workplace Neutron Fields – Part 1: Characteristics and Methods of Production. ISO, Geneve, pp. 12789–12791.
ISO. Passive Personal Neutron Dosimetry Systems. Performance and Test Requirements. In: ISO (Ed.), Geneva, in preparation.
Kluge, H., 1998. Irradiation Facility with Radioactive Reference Neutron Sources: Basic Principles. Ptb-Report. vol. PTB-N-34.
Kluge, H., Alevra, A.V., Jetzke, S., Knauf, K., Matzke, M., Weise, K., Wittstock, J., 1997. Scattered neutron reference fields produced by radionuclide sources. Radiation Protection Dosimetry 70 (1–4), 327–330.
Laughlin, J.S., Harvey, R.A., Haas, L.L., Lindsay, J.E., Beattie, J.W., 1951. Physical aspects of rotation therapy with the Betatron .1. American Journal of Roentgenology 65 (6), 947–951.
Miam, S.R.L., 2012. Politrack Automatic Track Detector Reader. http://www.miam.it/allegati_catalogo/BROCHURE%20POLITRACK%20ENGLISH.pdf.
NCRP, 2008. Uncertainties in the Measurement and Dosimetry of External Radiation Recommendations of the National Council on Radiation Protection and Measurements November 19, 2007. NCRP Report. National Council on Radiation Protection and Measurements, Bethesda, MD.
Sánchez-Doblado, F., Domingo, C., Gómez, F., Sánchez-Nieto, B., Muñiz, J.L., García-Fusté, M.J., Expósito, M.R., Barquero, R., Hartmann, G., Terrón, J.A., Pena4, J., Méndez, R., Gutiérrez, F., Guerre, F.X., Roselló, J., Núñez, L., Brualla-González, L., Manchado, F., Lorente, A., Gallego, E., Capote, R., Planes, D., Lagares, J.I., González-Soto, X., Sansaloni, F., Colmenares, R., Amgarou, K., Morales, E., Bedogni, R., Cano, J.P., Fernandez, F., 2012. Estimation of neutron-equivalent dose in organs of patients undergoing radiotherapy by the use of a novel online digital detector. Physics in Medicine and Biology 57, 6167–6191.
Seitz, F., 1958. On the theory of bubble chamber. Physics of Fluids 1 (1), 11.
Siebert, B.R.L., Schuhmacher, H., 1995. Quality factors, ambient and personal dose equivalent for neutrons, based on the new Icru stopping power data for protons and alpha particles. Radiation Protection Dosimetry 58 (3), 177–183.
Taylor, G.C., 2010. Geometry corrections for cylindrical neutron area survey meters. Applied Radiation and Isotopes 68 (4–5), 546–549.
Tommasino, L., Zapparoli, G., Spiezia, P., Griffith, R.V., Espinosa, G., 1984. Different etching processes of damage track detectors for personnel neutron dosimetry. Nuclear Tracks and Radiation Measurements 8 (1–4), 335–339.
Tosi, G., Torresin, A., Agosteo, S., Foglio Para, A., Sangiust, V., Zeni, L., Silari, M., 1991. Neutron measurements around medical electron accelerators by active and passive detection techniques. Medical Physics. 18 (1), 54–60.
Tume, P., Lewis, B.J., Bennett, L.G., Cousins, T., 1998. Characterisation of neutron-sensitive bubble detectors for application in the measurement of Jet aircrew exposure to natural background radiation. Nuclear Instruments and Methods in Physics Research A 406 (1), 153–168.
Vanhavere, F., Loos, M., Plompen, A.J.M., Wattecamps, E., Thierens, H., 1998. A combined use of the Bd-Pnd and Bdt bubble detectors in neutron dosimetery. Radiation Measurements 29 (5), 573–577.
Vanhavere, F., Thierens, H., Loos, M., 1996. Testing the temperature compensated Bd-Pnd bubble detector. Radiat Protection Dosimetry 65 (1–4), 425–428.
Waller, E.J., Jamieson, T.J., Cole, D., Cousins, T., Jammal, R.B., 2003. Experimental and computational determination of neutron dose equivalent around radiotherapy accelerators. Radiation Protection Dosimetry 107 (4), 225–232.
Wolff, D., Stieler, F., Welzel, G., Lorenz, F., Abo-Madyan, Y., Mai, S., Herskind, C., Polednik, M., Steil, V., Wenz, F., Lohr, F., 2009. Volumetric modulated arc therapy (Vmat) vs. Serial tomotherapy, step-and-shoot Imrt and 3d-Conformal Rt for treatment of prostate cancer. Radiotherapy and Oncology 93 (2), 226–233.
Zimbal, A., 2009, Personal Communication.
Zhou, D., Semones, E., Weyland, M., Benton, E.R., 2007. Let calibration for Cr-39 detectors in different oxygen environments. Radiation Measurements 42 (9), 1499–1506.
Zytkovicz, A., Daftari, I., Phillips, T.L., Chuang, C.F., Verhey, L., Petti, P.L., 2007. Peripheral dose in ocular treatments with cyberknife and gamma knife radiosurgery compared to proton radiotherapy. Physics in Medicine and Biology 52 (19), 5957–5971.